Ultra-Small-Angle X-ray Scattering—X-ray Photon Correlation Spectroscopy: A New Measurement Technique for *In-Situ* Studies of Equilibrium and Nonequilibrium Dynamics

F. ZHANG, A.J. ALLEN, L.E. LEVINE, J. ILAVSKY, and G.G. LONG

Ultra-small-angle X-ray scattering—X-ray photon correlation spectroscopy (USAXS-XPCS) is a new measurement technique for the study of equilibrium and slow nonequilibrium dynamics in disordered materials. This technique fills a gap between the accessible scattering vector ranges of dynamic light scattering (DLS) and XPCS. It also overcomes the limits of visible light scattering techniques imposed by multiple scattering and is suitable for the study of optically opaque materials containing near-micrometer-sized structures. In this article, we present an overview of the important technical aspects of USAXS-XPCS and offer a few examples as well as future outlooks to illustrate the capability of USAXS-XPCS for monitoring equilibrium and nonequilibrium dynamics.

DOI: 10.1007/s11661-011-0790-0

I. INTRODUCTION TO ULTRA-SMALL-ANGLE X-RAY SCATTERING–X-RAY PHOTON CORRELATION SPECTROSCOPY

STATIC scattering methods have long played an important role in developing our understanding of the structure of materials.[1,2] However, understanding the *dynamic* properties of materials has proven much more challenging and presents a grand challenge to the scientific community. Scattering-based techniques that cover a broad range of time and length scales have been developed to meet this challenge.[3] Among them are dynamic light scattering (DLS)[4] and X-ray photon correlation spectroscopy (XPCS),[5,6] two techniques that use the coherent properties of electromagnetic radiation to monitor the low-frequency dynamics of disordered systems.

DLS and XPCS share the same physical principle—constructive interference of scattered coherent light from a disordered system gives rise to a random scattering pattern (“speckle pattern”),[7] which, under the first-order Born approximation, can be related to density fluctuations within the sample provided that the phase and amplitude of the incident electromagnetic wave are known. The motion of the scatterers is reflected in the observed intensity fluctuations in the speckle patterns; dynamics of the sample system can be inferred by analyzing the temporal correlation of the speckle intensity. To establish the coherent interference, both techniques require the dimensions of the sampling volume to be within or similar to those associated with the longitudinal and transverse coherent lengths of the incident beam.

The main difference between DLS and XPCS resides in the wavelength of the electromagnetic radiation that is employed. DLS, as a light scattering technique, uses waves of much longer wavelength when compared with XPCS, an X-ray scattering technique. This difference leads to their respective advantages and disadvantages. Foremost, the magnitude of the scattering vector q is related to the wavelength λ following $q = (4\pi/\lambda)\sin(\theta)$, where 2θ is the scattering angle. The wavelength of visible light ranges from 4000 to 7000 Å, which restricts the light scattering to a range where q is very small ($q < 10^{-4}$ Å^{-1}). XPCS, with the shorter wavelength of X-rays (≈1 Å), typically measures the low frequency dynamics in a q range from 1×10^{-3} Å^{-1} up to several Å^{-1}.[3] DLS enjoys advantages for the availability of flexible optics and high brilliance and coherence laser sources, but the corrections for multiple scattering in DLS often prove challenging.[4] Consequently, it is difficult, if not impossible, to use visible light DLS to study the dynamics of optically opaque or highly absorbing samples. On the other hand, X-rays feature small scattering cross sections, which makes multiple scattering much less of a concern.

Although XPCS is basically a transposition of DLS into the X-ray regime, it was fully developed only after high-brilliance, partially coherent X-ray beams became available at third generation synchrotron sources.[8,9] An illustration of a typical XPCS instrument[10,11] is shown in Figure 1(a). The partially coherent X-ray beam from an undulator source is defined by a coherence-defining

F. ZHANG, Research Associate, National Institute of Standards and Technology, Gaithersburg, MD 20899, is also Adjunct Research Physicist, with the Northern Illinois University, DeKalb, IL 60115. A.J. ALLEN and L.E. LEVINE, Physicists, are with the Material Measurement Laboratory, National Institute of Standards and Technology. J. ILAVSKY, Physicist, is with the X-ray Science Division, Advanced Photon Source, Argonne National Laboratory, Argonne, IL 60439. Contact e-mail: ilavsky@aps.anl.gov G.G. LONG, Physicist, is with the X-ray Science Division, Advanced Photon Source, Argonne National Laboratory, and is also with the Material Measurement Laboratory, National Institute of Standards and Technology.

Manuscript submitted February 13, 2011.
Article published online September 13, 2011

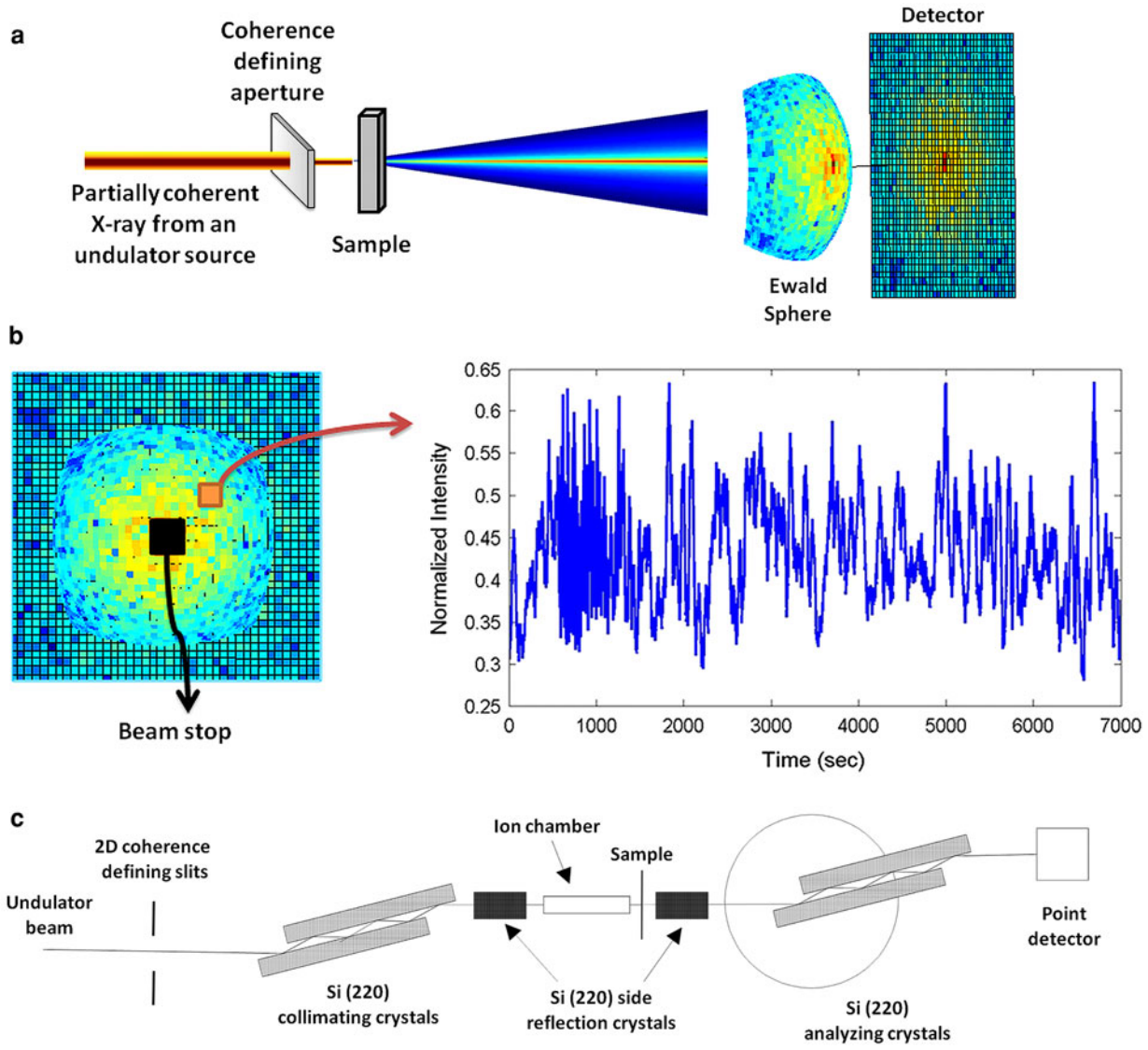

Fig. 1—(*a*) Illustration of coherent SAXS and the formation of speckle patterns. (*b*) Illustration of typical XPCS data. (*c*) Schematic of the USAXS-XPCS instrument.

aperture placed before the sample with a disordered local structure. The coherent speckle pattern on the Ewald sphere in the paraxial (small q) condition is readily collected by a two-dimensional charge-coupled device (CCD) detector.[5] At each fixed pixel, the intensity fluctuation is recorded as a function of time and analyzed to reveal the dynamic properties at the corresponding q. A typical XPCS plot of the time-dependent, normalized intensity for an equilibrium dynamic process is shown in Figure 1(b).

Although XPCS is a fairly recent technique, it has had a significant impact on many aspects of statistical physics and has provided access to a wide range of physical processes with low-frequency dynamics, such as equilibrium dynamics in colloidal dispersions;[12–15] critical fluctuations of liquid crystals near phase transitions;[16,17] and slow-varying, nonequilibrium dynamics in weakly disturbed soft matter systems[18–21] and alloys.[22,23] More details and applications of XPCS can be found in recent review articles.[3,5,6,24]

Inspection of the applicable q ranges of DLS and XPCS shows a gap between about 1×10^{-4} Å^{-1} and 1×10^{-3} Å^{-1}. This gap is similar to the one between conventional small-angle X-ray scattering (SAXS) and light scattering[25] and is normally buried behind the beamstop in SAXS experiments, as illustrated in Figure 1(b). A wide variety of microstructures in the size range from 1000 Å to several micrometers[26,27] is best studied in this q range, because this is the regime where $qD \approx 1$. Here, D is a representative dimension of the microstructure. Ultra-small-angle X-ray scattering–X-ray photon correlation spectroscopy (USAXS-XPCS) was developed[28] in response to this need.

Figure 1(c) shows a schematic of the USAXS-XPCS instrumentation, which is based at the USAXS facility[29] at the Advanced Photon Source, Argonne National

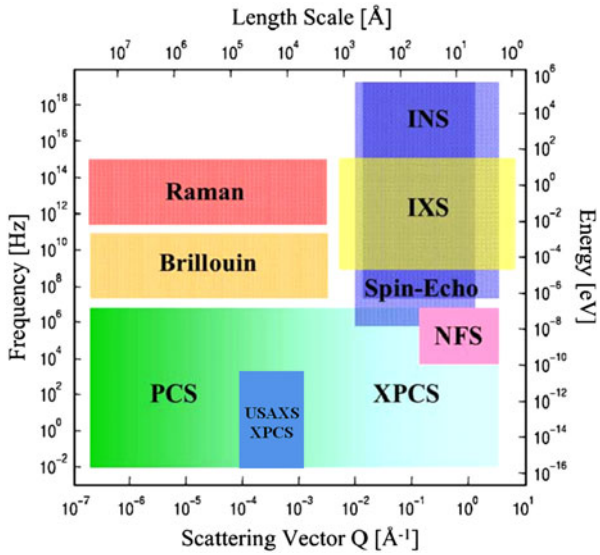

Fig. 2—Frequency–scattering wavevector domains of available techniques for dynamic studies (adapted and modified from Grübel and Zontone[3]). The techniques in the map are as follows: Raman spectroscopy, Brillouin spectroscopy, inelastic neutron scattering, inelastic X-ray scattering, neutron spin-echo spectroscopy, nuclear forward scattering, XPCS, USAXS-XPCS, and DLS (also known as photon correlation spectroscopy (PCS)).

Laboratory. Compared with the illustration of typical XPCS instrumentation in Figure 1(a), USAXS-XPCS has two pairs of parallel double-crystals oriented in both transverse directions. These highly polished Si (220) crystal optics, with their narrow Darwin curves (full-width at half-maximum ≈ 15.36 μrad for 10 keV X-rays), enable the coherent scattering intensity within the aforementioned q gap to be probed. Other advantages of crystal optics include enhanced longitudinal coherence of the partially coherent X-rays,[28] reduction of the parasitic scattering,[30] and preservation of the coherence of monochromatic X-rays due to the nondispersive configuration of the crystal optics.[31]

The intrinsic time resolution of USAXS-XPCS is limited by two factors: the time resolution of the detector and the coherent scattering intensity at the detector. Currently, two detectors are available for USAXS-XPCS: a low-noise scintillation detector with a time resolution of 1×10^{-3} seconds and a photodiode detector with a time resolution of 0.1 seconds. Time resolution comparable to the detector time resolution can be achieved in studies of equilibrium dynamics. With the scattering q range and the time resolution of USAXS-XPCS, we modified the frequency–scattering wavevector domain map of available techniques for dynamic studies (Figure 2). This modification is based on the original map found in Grübel and Zontone.[3] USAXS-XPCS was already demonstrated in the q range of 1×10^{-4} Å^{-1} to 1×10^{-3} Å^{-1}. This capability could be expanded toward the high-q or high frequency side of the spectra by using a source that can generate more coherent X-ray flux, such as free-electron laser or energy recovery linear accelerator (LINAC) sources.

II. USAXS-XPCS FOR STUDIES OF EQUILIBRIUM DYNAMICS

Equilibrium is the state of matter in which the forward rates of processes equal the reverse rates for the same processes. A full understanding of thermally-induced equilibrium dynamics is of great importance to materials research, especially those of soft material, which is easily affected by thermal stresses or thermal fluctuations. Soft materials, *e.g.*, polymers, proteins, *etc.*, share some common traits. Their thermally-induced physical behaviors occur at an energy level comparable to the thermal energy associated with room temperature, which makes quantum effects irrelevant.[1] The small energy involved also dictates that the fluctuation must be slow. Meanwhile, soft materials frequently have physical structures much larger than the atomic or molecular scale, and yet much smaller than the macroscopic dimension of the material. These features make USAXS-XPCS a highly relevant technique for probing the dynamics of such materials due to its applicable frequency and q range.

As with conventional XPCS, USAXS-XPCS probes equilibrium dynamics by monitoring the intensity fluctuation at a fixed q. This measurement is implemented by keeping the sample, optics, and detector stationary, while measuring the count rate of the detector continuously. The primary quantity obtained in such measurements is the normalized, time-averaged, second-order intensity autocorrelation function:

$$g_2(q,t) = \frac{\langle I(q,t+t')I(q,t')\rangle_E}{\langle I(q,t')\rangle_E^2} \qquad [1]$$

Here, $I(q,t)$ is the integrated scattering intensity in an interval Δt around a time t at a fixed q, and the angular brackets in Eq. [1] denote an ensemble average. In USAXS-XPCS measurements, $I(q,t)$ is the detector intensity normalized by the intensity obtained in an ion chamber placed immediately in front of the sample. Previous autocorrelation analyses showed that normalization has a negligible effect on $g_2(q,t)$.[28] Following Eq. [1], for $t' \to \infty$, $g_2(q,t) \to 1$; and for $t' \to 0$, $g_2(q,t) \to 1 + \beta$, where β, known as the coherence factor or optical contrast, varies between 0 and 1 and accounts for the smearing introduced by scattering from a volume larger than one coherence. Mathematically, β is the variance of the intensity fluctuation normalized by $\langle I(q,t')\rangle_E^2$. For perfectly coherent light, $\beta = 1$. For partially coherent X-rays used in USAXS-XPCS measurements at third generation X-ray sources, β is on the order of 0.1.

Depending on the sample system, $g_2(q,t)$ is capable of revealing different underlying physics. For instance, when the scattering volume contains a large number of independent scatterers that undergo thermal motion in equilibrium, according to the central limit theorem, the temporal fluctuations in the coherent scattering intensity obey Gaussian statistics and $g_2(q,t)$ fully describes the correlation spectrum. As such, the intensity autocorrelation function is related to the intermediate scattering function of the sample following the Siegert relation:[7]

$$g_2(q,t) = 1 + \beta |f(q,t)|^2 \quad [2]$$

where $f(q,t) = S(q,t)/S(q)$ is the intermediate scattering function, with $S(q)$ and $S(q,t)$ being the initial structure factor and that after time t, respectively. The intermediate scattering function in the time domain is the normalized dynamic structure factor, a fundamental parameter in the description of the dynamic behavior of condensed matter that can also be acquired with inelastic scattering, depending on both time and q. The dynamic structure factor is related to the time-dependent Fourier transform of the pair correlation function and is often the key for successful comparison of theory with experiment.

For scatterers undergoing thermally induced free diffusion (Brownian motion), the intensity autocorrelation function follows a simple exponential form:

$$g_2(q,t) = 1 + \beta \exp(-2\Gamma t) \quad [3]$$

where Γ is the relaxation rate and is related to the diffusion constant D_0 of the scatterers following the Stokes–Einstein relation $\Gamma = D_0 q^2$, assuming that the scatterers are monodisperse in size.

When the interaction between the scatterers cannot be ignored, the dynamics are often collective, and the assumption for Eq. [3] (free diffusion) is violated. Dynamic studies show that a slow, hyperdiffusive motion can be characterized by an empirical correlation function, also known as the Kohlrausch–Williams–Watts (KWW) function:[15]

$$g_2(q,t) = 1 + \beta \exp(-2 \times (\Gamma t)^{\gamma}) \quad [4]$$

Here, γ is an exponent (the Kohlrausch exponent), which, when greater than 1, indicates a decay that is compressed and faster than that expected from particles under Brownian motion ($\gamma = 1$) and *vice versa*. This function has been widely applied to studies of viscoelastic systems with DLS[32] and XPCS.[33]

USAXS-XPCS is capable of revealing aspects of the equilibrium dynamics associated with Eqs. [2] through [4]. In the rest of this section, we present an example of colloidal suspensions undergoing collective motion, which represents the most complex aspect of all three.

A sample was prepared from an aqueous colloidal suspension of polystyrene (PS) microspheres (Thermal Scientific Inc.,* Fremont, CA), which have a narrow Gaussian-type size distribution in diameter. The measured mean diameter of the PS microspheres, obtained from a USAXS analysis, was ≈10,170 Å, and its Gaussian width was ≈260 Å. Both to slow the dynamics and increase the scattering contrast, the PS spheres were transferred to a glycerol/water mixture (glycerol mass fraction: ≈0.97). The final volume fraction of PS spheres in the suspension was ≈10 pct. USAXS-XPCS measurements were carried out with coherence-defining slits set at 15 μm × 15 μm and an X-ray energy at 10.5 keV (X-ray wavelength: 1.18 Å), with q fixed at 0.00015, 0.0003, 0.0004, 0.0005, 0.0006, and 0.0007 Å^{-1}. The temperature of the colloidal dispersion was 278.15 K (5 °C), and the measurement time at each q was approximately 1400 seconds.

The intensity autocorrelation functions normalized by the optical contrast are shown in Figure 3 for time delays from 1 to 100 seconds. It is evident that faster dynamics is associated with larger scattering vector q. This phenomenon is expected considering that the short-range fluctuations (large q) occur more rapidly than long-range fluctuations (small q) in interacting colloidal dispersions. Similar to Gutt *et al.*,[34] we identified small fluctuations in the long time-delay end of the autocorrelation functions, which can be attributed to the partial coherence of the beam and the limited detector resolution.

The intensity autocorrelation functions were analyzed with Eq. [4] to extract the relaxation time constant τ, which is the inverse of the relaxation rate Γ. At all q values, the KWW exponent γ was greater than 1, signifying that the motion of the PS microspheres is at least partially collective in nature. As shown in Figure 4, the relaxation time τ shows a monotonic decay as q increases, which reflects the slower dynamics of larger length scales. This trend is qualitatively similar to the observation of silica nanoparticles in 1,2 propanediol, another viscous fluid.[15] Interestingly, these results are different from those of a previous XPCS study of a similar system [PS spheres with nominal radius 665 Å in glycerol at 268 K (−5 °C)].[35] In that system, the authors found that the intensity autocorrelation functions followed a simple exponential decay ($\gamma = 1$) for suspensions with PS volume concentration as high as 28 pct, which suggests that despite the apparent high level of concentration, the interparticle interaction did

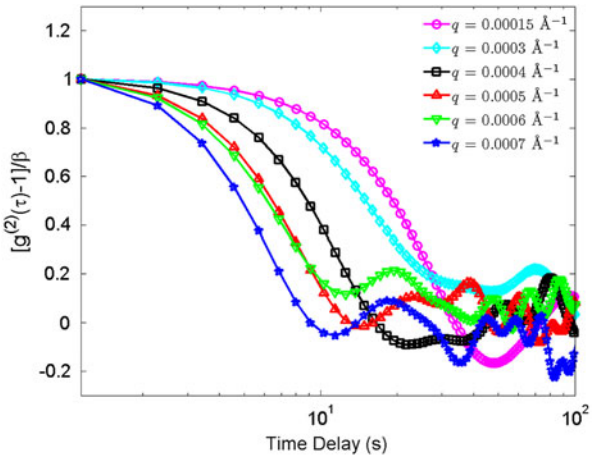

Fig. 3—Normalized intensity autocorrelation functions measured at $q = 0.00015$ Å^{-1}, $q = 0.0003$ Å^{-1}, $q = 0.0004$ Å^{-1}, $q = 0.0005$ Å^{-1}, $q = 0.0006$ Å^{-1}, and $q = 0.0007$ Å^{-1}, for 10 vol pct PS microspheres in a glycerol/water mixture. The one sigma confidences are smaller than the symbols for the points.

*Certain trade names and company products are mentioned in the text or identified in illustrations in order to specify adequately the experimental procedure and equipment used. In no case does such identification imply recommendation or endorsement by National Institute of Standards and Technology, nor does it imply that the products are necessarily the best available for the purpose.

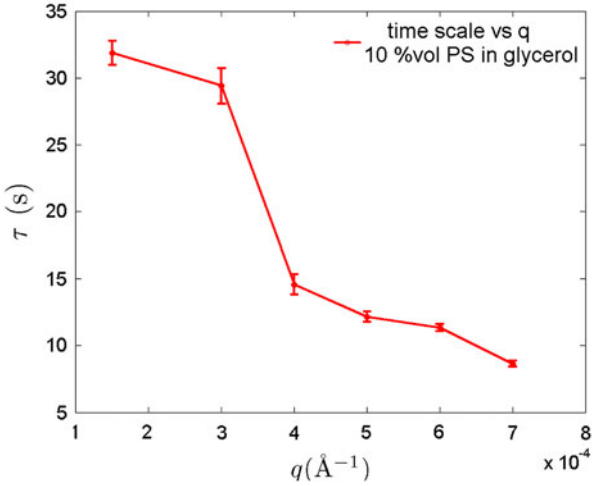

Fig. 4—Relaxation time of a 10 pct PS dispersion in a glycerol/water mixture as a function of q.

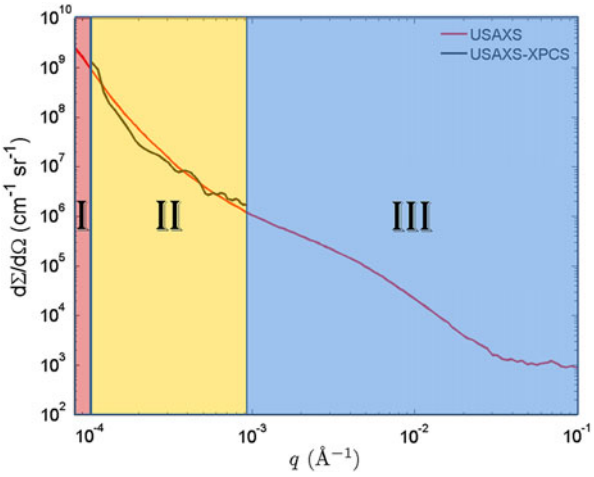

Fig. 5—Comparison of the USAXS and USAXS-XPCS curves. The sample was a sil-ACP composite sample. The measurements were conducted at 398.15 K (125 °C). Zones I, II, and III represent the q range that can be probed by DLS, USAXS-XPCS, and conventional XPCS, respectively.

not significantly disrupt the free diffusion of the particles. The USAXS-XPCS results shown in Figures 3 and 4 suggested otherwise. We observed hyperdiffusive behavior ($\gamma > 1$) of the PS microspheres in the measured q range at volume concentrations as low as 10 pct. We note that this type of dependence of the Kohlrausch exponent γ on q was also observed in a study of nanoparticle motion in polymer melts, where in a large-q region, the nanoparticles follow Brownian-type diffusive motion and in a small-q region KWW-form hyperdiffusive motion.[36] We speculate that our observations may be related to the dependence of the hydrodynamic interaction on q in many-body colloidal systems,[14] which is affected by the change of the strength of the hydrodynamic interaction caused by local density gradients.

III. USAXS-XPCS FOR STUDIES OF NONEQUILIBRIUM DYNAMICS

Our most powerful theories for understanding the behavior of complex systems, thermodynamics and statistical mechanics, are largely limited to systems that are in equilibrium. Attempts to extend these theories to nonequilibrium conditions were only partially successful, and there exists a largely unsatisfied need for new experimental probes that can quantify the microscopic behavior of complex systems as they approach equilibrium. Accurate predictions and measurements of such behavior will not only address major difficulties in bridging theories across many length and time scales but also promise significant technological payoffs including control and optimization of material properties and formation.

USAXS-XPCS, as an interferometric measurement technique using short-wavelength X-rays, is capable of revealing the dynamic time scale of the nonequilibrium process in the appropriate time and length scales. In contrast to the fixed-q measurement mode that is suitable for the study of equilibrium dynamics, a scan measurement mode of USAXS-XPCS can be adopted for studying nonequilibrium dynamics that occurs when a material is disturbed and approaches equilibrium slowly. In this mode, the scattering vector q is scanned along the vertical (y) direction within a limited q_y range by rotating the analyzer crystals (Figure 1(c)), while the horizontal q_x is fixed at 0. A typical USAXS-XPCS curve as well as its corresponding USAXS curve is shown in Figure 5. While the USAXS curve is smooth over the entire q range, the USAXS-XPCS curve shows clear ''bumpy'' features that are introduced by coherent interference of the X-rays in its limited q range. In a static condition, this scan captures the form of the static X-ray speckles from the scattering volume, which is related by a Fourier transform to the exact microstructure in the scattering volume.[37] When the system undergoes slow dynamic changes, the local structure within the scattering volume produces corresponding changes in the speckle pattern that can be readily followed by repeated scans using the USAXS-XPCS scan mode. Because this scan measurement mode requires rotational movement of the analyzer crystals, the time resolution of the scan measurement mode is poorer than that of the fixed-q measurement mode. The best time resolution that can be achieved with the current instrument is ≈60 seconds. For the speckle pattern to remain approximately stable during each USAXS-XPCS scan, the time scale of the probed dynamics must be significantly longer than this ≈60 seconds time resolution. We also note that the point-detection nature of USAXS-XPCS prohibits us from obtaining simultaneously the scattering intensities at different q values; thus, metrics such as two-time correlation functions.[38] are inapplicable since they require averaging ensembles of intensities over a range of scattering vectors.

We also point out that the time-averaged intensity autocorrelation analysis in the previous section makes a

fundamental assumption that the dynamics is stationary over the duration of the measurement; hence, no information is lost by performing a time average of the measured intensities. This assumption breaks down for nonequilibrium dynamics. To overcome this challenge and monitor the rate of change in the sample system that is revealed by the evolution of USAXS-XPCS scans, we developed an analysis method based on the correlation coefficient, which is a simple scalar statistical parameter that describes the degree of resemblance between two datasets. The correlation coefficient $\phi(i, j)$ is defined as

$$\phi(i,j) = \frac{C(i,j)}{\sqrt{C(i,i)C(j,j)}} \quad [5]$$

where i and j represent the ith and jth dataset, and $C(i,j)$ is the covariance of variables i and j, which follows the standard statistical definition $C(i,j) = \langle (i - \langle i \rangle) \times (j - \langle j \rangle) \rangle$, in which $\langle \ldots \rangle$ represents the statistical mean. Following this definition, when datasets i and j are identical, the correlation coefficient is 1. This method is similar to the one used in the statistical analysis of the evolution of coherent, quasi-static X-ray speckles of the magnetic domains in a magnetic film as a function of the applied magnetic field.[39]

In our analysis, the datasets i and j in Eq. [5] are obtained from the measured USAXS-XPCS intensities from the q scan. One prominent characteristic of USAXS-XPCS data in the scan measurement mode is that the coherent scattering intensity normally spans over two orders of magnitude in scattering intensity. To give each data point equal weight in a statistical analysis, we normalize the USAXS-XPCS intensity with the corresponding, separately measured, USAXS intensity. This USAXS scan is identical to the USAXS-XPCS scans described previously, except that the scattering volume is made much larger than the coherence volume. Thus, no speckles are observed, and only the volume-averaged q behavior is obtained.

Another small-sample-size effect that must be compensated for is the sensitivity of USAXS-XPCS scans to small fluctuations in the apparent sample transmission (*e.g.*, from small changes in the incident beam). In order to compensate for these effects, each of the USAXS-XPCS and USAXS datasets are self-normalized using a function analogous to the small-angle scattering invariant, a parameter commonly used in small-angle scattering data analysis to derive the total volume fraction of the scatterers. These normalization procedures allow the normalized intensities to carry the same weight through the q range and be independent of any possible changes in the scattering volume, and provide the required datasets i and j for Eq. [5]. Further details of this analysis method can be found elsewhere.[28,40]

Using the correlation coefficient analysis described previously, we have studied a series of hard condensed matter systems that approach equilibrium *via* slowly evolving nonequilibrium dynamics. In the remainder of this section, we will use two examples to illustrate the capability of USAXS-XPCS to reveal dynamic time scales of nonequilibrium dynamic processes.

We use a simple example of a two-dimensional correlation coefficient map (Figure 6) to demonstrate its potential in assessing USAXS-XPCS data. The sample used for this measurement was an amorphous calcium phosphate (ACP) based composite that is used as a self-repairing dental material.[41,42] The ACP particles were coated with silane groups to enhance surface binding with a (2, 2-bis[(p-2'-hydroxy-3'-methacryloxypropoxy)phenyl]propane (Bis-GMA) and triethyleneglycol dimethacrylate (TEGDMA) polymer matrix as a means of increasing the mechanical strength of the composite. The USAXS-XPCS data were acquired in the scan measurement mode with a 15 μm × 15 μm, 10.5 keV partially coherent X-ray beam during sample cooling from 398.15 K to 298.15 K (125 °C to 25 °C), after the sample was annealed at a temperature of 398.15 K (125 °C) for ≈200 minutes. Figure 6 shows the correlation coefficient from every possible pair of data. The X-axis of the figure shows the start acquisition time of the ith USAXS-XPCS scan, as in Eq. [5], and the Y-axis shows the start acquisition time of the jth USAXS-XPCS scan. The color scale, displayed to the right of the figure, shows the magnitude of the correlation coefficient following Eq. [5]. The higher the value is, the more correlated the ith and jth scans are. A feature of this type of analysis is that as the sample approaches an equilibrium state, successive scans become highly correlated with each other. This is represented by the triangular red region toward the upper-right side of the plot. The dynamic time scale corresponding to the underlying nonequilibrium process therefore can be readily acquired, as shown by the dashed line in the figure. In addition, Figure 6 reveals that during cooling, the microstructural evolution of the sil-ACP composite resembles a two-step process. In the initial state (0 to 30 minutes), very little change occurred in the local microstructure. The transformation to a second state occurred at ≈30 minutes (dotted line). After this transformation, the USAXS-XPCS patterns

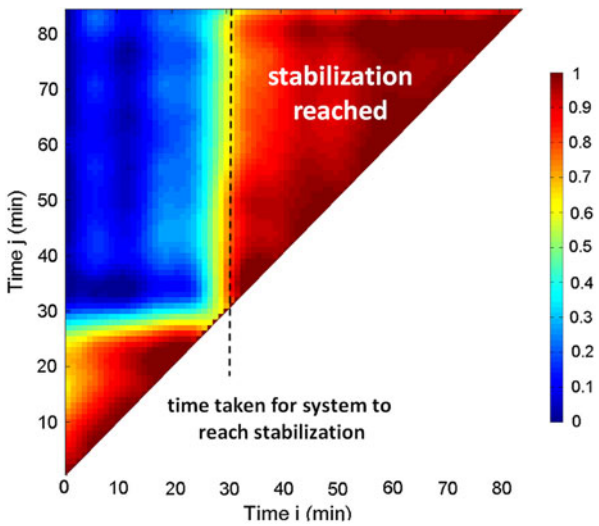

Fig. 6—Correlation coefficient map for sil-ACP during cooling from 398.15 K to 298.15 K (125 °C to 25 °C).

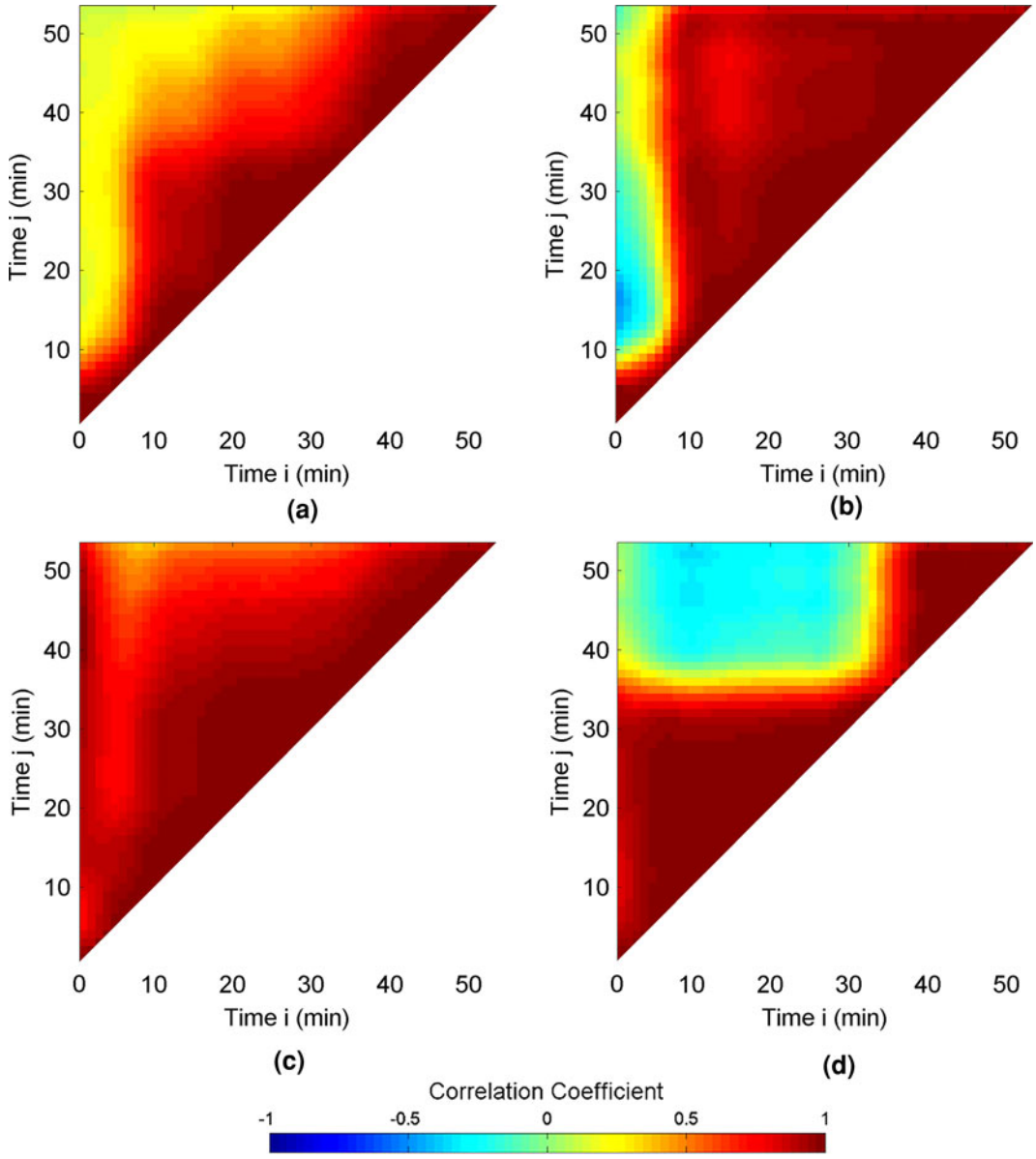

Fig. 7—Correlation coefficient maps for glass composites following heating to 388.15 K (115 °C) from 298.15 K (25 °C) for q ranges of (*a*) 2×10^{-4} Å^{-1} to 8×10^{-4} Å^{-1}, (*b*) 2×10^{-4} Å^{-1} to 4×10^{-4} Å^{-1}, (*c*) 4×10^{-4} Å^{-1} to 6×10^{-4} Å^{-1}, and (*d*) 6×10^{-4} Å^{-1} to 8×10^{-4} Å^{-1}.

became and remained highly correlated until the end of the measurement. For this simple example, Figure 6 illustrates how the dynamic time scale associated with a nonequilibrium local-microstructure change can be revealed by USAXS-XPCS. We note that to monitor the nonequilibrium dynamics of this system in response to an external stimulus, an isothermal condition is required, *e.g.*, the condition to acquire the data for Figure 7.

Scan mode USAXS-XPCS is also capable of revealing dynamics occurring within a narrow q range; Figure 7 shows an example of this capability. The glass composite sample used for this study contained barium boron aluminum silicate glass fillers embedded in a Bis-GMA and TEG-DMA polymer matrix. The measurements under isothermal conditions were taken immediately after the sample temperature was increased to 388.15 K (115 °C) from room temperature [≈298 K (25 °C)]. This temperature is above the glass transition temperature of the polymer matrix making it a highly viscous medium. Figure 7(a), which represents the correlation coefficient map for the USAXS-XPCS data in the q range of 2×10^{-4} Å^{-1} to 8×10^{-4} Å^{-1}, suggests that a rather complicated dynamic process occurred in the sample on its way to equilibrium. However, a closer examination of the USAXS-XPCS data in three equal-spaced sub-q ranges (2×10^{-4} Å^{-1} to 4×10^{-4} Å^{-1} (Figure 7(b)); 4×10^{-4} Å^{-1} to 6×10^{-4} Å^{-1} (Figure 7(c)); and 6×10^{-4} Å^{-1} to 8×10^{-4} Å^{-1} (Figure 7(d))) suggests that the underlying dynamics could be relatively simple. While the correlation map in the intermediate range remains highly correlated throughout the duration of

the measurement, the correlation maps in the small-q and large-q ranges show behaviors that resemble that of Figure 6. An analysis of the USAXS profile of this sample shows a bimodal size distribution of the glass fillers with the nominal size of the larger population approximately tripling that of the smaller population (data not shown). Taking this information into account, Figure 7 shows that after heating, the low-q region reached stabilization ≈6 times more quickly than the high-q region. The driver for this nonequilibrium dynamics is the isothermal relaxation of the nonuniform stress caused by the thermal mismatch between the filler particles and the polymer matrix during the heating process. Small changes in the positions and dimensions of the larger particles cause positional shifts of the smaller particles that are significant compared with their size. Thus, the high-q scattering region cannot reach equilibrium before the low-q region stabilizes. In addition, there is an inherent difference in sensitivity. Thus, a fixed displacement of the polymer introduces a larger relative phase shift for the embedded smaller particles (corresponding to high-q scattering) than for the embedded larger particles (corresponding to low-q scattering). Therefore, the correlation coefficient map in the low-q region reaches its final equilibrium state faster than that in the high-q region; and the complicated features in Figure 7(a) are explained.

IV. CONCLUSIONS AND OUTLOOK

In this article, we have provided an overview of USAXS-XPCS as a dynamic approach to filling the gap between DLS and conventional XPCS in the time/frequency–scattering vector/length scale domains of the available techniques. The interferometric nature of USAXS-XPCS makes this technique sensitive enough to monitor subtle local structural changes. Compared with conventional XPCS, USAXS-XPCS relies on Bonse–Hart type crystal optics to access the q range that is ''behind the beamstop'' and is a point-detection technique. This attribute is partially responsible for the limited time resolution of USAXS-XPCS (≈0.001 seconds in the fixed-q mode and 60 seconds in the scan mode). However, the suitable q range of USAXS-XPCS corresponds to large structures (≈1000 Å to ≈1 μm) whose dynamics are inherently slow. Therefore, the limited time resolution does not present major problems in detecting the slow dynamics from large structures.

USAXS-XPCS in the fixed-q mode provides a good measure of equilibrium dynamics. Due to the small scattering cross section of X-rays, USAXS-XPCS has a major advantage over DLS for investigating optically opaque samples. Suitable sample systems are common in the confines of soft materials—various polymer solutions and blends, organic and biological micelles, and colloidal dispersions all have microstructural length scales consistent with the q range of USAXS-XPCS.[26]

For example, while the dynamics of single-component colloidal dispersions were gradually unveiled by means of XPCS and DLS, the dynamics of two- or multicomponent colloidal dispersions are not yet fully understood. Unexpected behaviors such as the existence of attractive interactions between hard-sphere colloidal particles of different sizes mediated within a liquid suspension were reported.[43] USAXS-XPCS, due to its accessible q range, can improve our understanding of the underlying interaction that governs the equilibrium dynamics of binary colloidal mixtures of large[44] and small size ratios[45] (*i.e.*, whether it is a strong and short-range attraction or relatively long-range repulsion between these colloids). It is also known that the dynamics of soft materials is often size dependent, for example, the dynamics of nanoparticles[46] and micelles[47] in polymer melts. In this respect, USAXS-XPCS is a complementary technique to both DLS and XPCS to map the complete dynamic structure factor of these systems.

In the scan measurement mode, USAXS-XPCS provides an opportunity for studying the dynamic behavior and revealing the dynamic time scale associated with slowly evolving nonequilibrium dynamics. For example, in a previous study, we established the temperature-dependent dynamic time scales of ACP-based composites and found an activation energy related to the loss of water in these composites *via* an Arrhenius analysis.[40]

Finally, we note that nonequilibrium phenomena are also pervasive in hard materials where they are critically important for the control of material processes and properties. Currently, a study is underway on ''transformation induced plasticity'' (TRIP) steels, one of the newest and most exciting materials being developed by the steel industry.[48] TRIP steels exhibit a rich phase behavior and have better ductility at a given strength level when compared with other high-strength steels. The combined USAXS and USAXS-XPCS study is expected to reveal local and overall changes in the microstructure that are related to the diffusion of carbon in the system and the transformation between austenites and martensites as a function of temperature.

Cement and concrete form another important class of hard materials where USAXS-XPCS measurements could play a key role. For example, alkali-activated slag (AAS) cement systems are of increasing interest due to the potential reduction in CO_2 emission during cement manufacture if some of the cement can be replaced by slag (a waste product from steel manufacture). However, the ability of AAS cements to resist chemical attack and carbonation over extended time scales must be carefully monitored.[49] The scan mode of USAXS-XPCS would allow the early onset of incipient damage effects due to carbonation to be explored and quantified.

USAXS-XPCS is a technique that was recently developed and implemented. While the applicable frequency and wave-vector range of USAXS-XPCS are limited, it is a unique tool for following the slow dynamics in disordered and optically opaque materials. Furthermore, with the introduction of fourth generation synchrotron sources, the time resolution of USAXS-XPCS will be improved and its q range will be expanded. It is anticipated that this technique will be important in the understanding of thermally-induced equilibrium dynamics of soft materials and nonequilibrium behavior of both soft and hard materials, and lead to technical payoffs in a wide range of areas such as the manufacture

of advanced ceramic and metallurgical materials and self-repairing biologically critical materials.

ACKNOWLEDGMENTS

We thank J.M. Antonucci, D. Skrtic, and J.N.R. O'Donnell, NIST's Polymers Division, for preparing the dental composite samples. ChemMatCARS Sector 15 is principally supported by the National Science Foundation/Department of Energy under Grant No. NSF/CHE-0822838. Use of the Advanced Photon Source, an Office of Science User Facility operated for the United States Department of Energy (U.S. DOE) Office of Science by Argonne National Laboratory, was supported by the U.S. DOE under Contract No. DE-AC02-06CH11357.

REFERENCES

1. P.M. Chaikin and T.C. Lubensky: *Principles of Condensed Matter Physics*, Cambridge University Press, Cambridge, United Kingdom, 2000.
2. A.J. Allen: *J. Am. Ceram. Soc*., 2005, vol. 88, pp. 1367–81.
3. G. Grübel and F. Zontone: *J. Alloys Compd*., 2004, vol. 362, pp. 3–11.
4. B.J. Berne and R. Pecora: *Dynamic Light Scattering: With Applications to Chemistry, Biology, and Physics*, Dover Publications, Inc., Mineola, New York, NY, 2000.
5. F. Livet: *Acta Crystallogr. Sect. A*, 2007, vol. 63, pp. 87–107.
6. M. Sutton: *Comptes Rendus Phys*., 2008, vol. 9, pp. 657–67.
7. J.W. Goodman: *Statistical Optics*, Wiley-Interscience, New York, NY, 1985.
8. M. Sutton, S.G.J. Mochrie, T. Greytak, S.E. Nagler, L.E. Berman, G.A. Held, and G.B. Stephenson: *Nature*, 1991, vol. 352, pp. 608–10.
9. S.B. Dierker, R. Pindak, R.M. Fleming, I.K. Robinson, and L. Berman: *Phys. Rev. Lett*., 1995, vol. 75, pp. 449–52.
10. D.L. Abernathy, G. Grübel, S. Brauer, I. McNulty, G.A. Stephenson, S.G.J. Mochrie, A.R. Sandy, N. Mulders, and M. Sutton: *J. Synchrotron Rad*., 1998, vol. 5, pp. 37–47.
11. A.R. Sandy, L.B. Lurio, S.G.J. Mochrie, A. Malik, G.B. Stephenson, J.F. Pelletier, and M. Sutton: *J. Synchrotron Rad*., 1999, vol. 6, pp. 1174–84.
12. T. ThurnAlbrecht, W. Steffen, A. Patkowski, G. Meier, E.W. Fischer, G. Grübel, and D.L. Abernathy: *Phys. Rev. Lett*., 1996, vol. 77, pp. 5437–40.
13. L.B. Lurio, D. Lumma, A.R. Sandy, M.A. Borthwick, P. Falus, S.G.J. Mochrie, J.F. Pelletier, M. Sutton, L. Regan, A. Malik, and G.B. Stephenson: *Phys. Rev. Lett*., 2000, vol. 84, pp. 785–88.
14. A.J. Banchio, J. Gapinski, A. Patkowski, W. Haussler, A. Fluerasu, S. Sacanna, P. Holmqvist, G. Meier, M.P. Lettinga, and G. Nagele: *Phys. Rev. Lett*., 2006, vol. 96, p. 138303.
15. C. Caronna, Y. Chushkin, A. Madsen, and A. Cupane: *Phys. Rev. Lett*., 2008, vol. 100, p. 055702.
16. A. Poniewierski, R. Holyst, A.C. Price, L.B. Sorensen, S.D. Kevan, and J. Toner: *Phys. Rev. E*, 1998, vol. 58, pp. 2027–40.
17. A. Madsen, J. Als-Nielsen, and G. Grübel: *Phys. Rev. Lett*., 2003, vol. 90, p. 085701.
18. R. Bandyopadhyay, D. Liang, H. Yardimci, D.A. Sessoms, M.A. Borthwick, S.G.J. Mochrie, J.L. Harden, and R.L. Leheny: *Phys. Rev. Lett*., 2004, vol. 93, p. 228302.
19. B. Chung, S. Ramakrishnan, R. Bandyopadhyay, D. Liang, C.F. Zukoski, J.L. Harden, and R.L. Leheny: *Phys. Rev. Lett*., 2006, vol. 96, p. 228301.
20. A. Robert, E. Wandersman, E. Dubois, V. Dupuis, and R. Perzynski: *Europhys. Lett*., 2006, vol. 75, pp. 764–70.
21. X.H. Lu, S.G.J. Mochrie, S. Narayanan, A.R. Sandy, and M. Sprung: *Phys. Rev. Lett*., 2008, vol. 100, p. 045701.
22. A. Malik, A.R. Sandy, L.B. Lurio, G.B. Stephenson, S.G.J. Mochrie, I. McNulty, and M. Sutton: *Phys. Rev. Lett*., 1998, vol. 81, pp. 5832–35.
23. F. Livet, F. Bley, R. Caudron, E. Geissler, D. Abernathy, C. Detlefs, G. Grübel, and M. Sutton: *Phys. Rev. E*, 2001, vol. 63, p. 036108.
24. K.A. Nugent: *Adv. Phys*., 2010, vol. 59, pp. 1–99.
25. A.J. Allen, P.R. Jemian, D.R. Black, H.E. Burdette, R.D. Spal S. Krueger, and G.G. Long: *Nucl. Instrum. Meth. Phys. Res. Sect. A*, 1994, vol. 347, pp. 487–90.
26. F. Zhang and J. Ilavsky: *Polymer Rev*., 2010, vol. 50, pp. 59–90.
27. T. Narayanan: *Curr. Opin. Coll. Interface Sci*., 2009, vol. 14, pp. 409–15.
28. F. Zhang, A.J. Andrew, L.E. Levine, J. Ilavsky, G.G. Long, and A.R. Sandy: *J. Appl. Crystallogr*., 2011, vol. 44, pp. 200–12.
29. J. Ilavsky, P.R. Jemian, A.J. Allen, F. Zhang, L.E. Levine, and G.G. Long: *J. Appl. Crystallogr*., 2009, vol. 42, pp. 469–79.
30. M. Sztucki, J. Gorini, J.-P. Vassalli, L. Goirand, P. van Vaerenbergh, and T. Narayanan: *J. Synchrotron Rad*., 2008, vol. 15, pp. 341–49.
31. D. Petrascheck: *Physica B & C*, 1988, vol. 151, p. 171.
32. F. Scheffold and P. Schurtenberger: *Soft Mater*., 2003, vol. 1, pp. 139–65.
33. L. Cipelletti and L. Ramos: *J. Phys.: Condens. Mater*., 2005, vol. 17, pp. R253–R285.
34. C. Gutt, T. Ghaderi, M. Tolan, S.K. Sinha, and G. Grübel: *Phys. Rev. B*, 2008, vol. 77, p. 094133.
35. D. Lumma, L.B. Lurio, M.A. Borthwick, P. Falus, and S.G.J. Mochrie: *Phys. Rev. E*, 2000, vol. 62, pp. 8258–69.
36. H.Y. Guo, G. Bourret, M.K. Corbierre, S. Rucareanu, R.B. Lennox, K. Laaziri, L. Piche, M. Sutton, J.L. Harden, and R.L. Leheny: *Phys. Rev. Lett*., 2009, vol. 102, p. 075702.
37. J.W. Miao, P. Charalambous, J. Kirz, and D. Sayre: *Nature*, 1999, vol. 400, pp. 342–44.
38. D. Lumma, L.B. Lurio, S.G.J. Mochrie, and M. Sutton: *Rev. Sci. Instrum*., 2000, vol. 71, pp. 3274–89.
39. M.S. Pierce, R.G. Moore, L.B. Sorensen, S.D. Kevan, O. Hellwig, E.E. Fullerton, and J.B. Kortright: *Phys. Rev. Lett*., 2003, vol. 90, p. 175502.
40. F. Zhang, A.J. Allen, L.E. Levine, L. Espinal, J.M. Antonucci, D. Skrtic, J.N.R. O'Donnell, and J. Ilavsky: *J. Biomed. Mater. Res*., 2011, submitted.
41. D. Skrtic and J.M. Antonucci: *Biomaterials*, 2003, vol. 24, pp. 2881–88.
42. D. Skrtic, J.M. Antonucci, E.D. Eanes, and N. Eldelman: *Biomaterials*, 2004, vol. 25, pp. 1141–50.
43. M.H.G. Duits, R.P. May, A. Vrij, and C.G. Dekruif: *J. Chem. Phys*., 1991, vol. 94, pp. 4521–31.
44. F. Zhang, G.G. Long, P.R. Jemian, J. Ilavsky, V.T. Milam, and J.A. Lewis: *Langmuir*, 2008, vol. 24, pp. 6504–08.
45. B.J. Anderson, V. Gopalakrishnan, S. Ramakrishnan, and C.F. Zukoski: *Phys. Rev. E*, 2006, vol. 73, p. 031407.
46. C.A. Grabowski, B. Adhikary, and A. Mukhopadhyay: *Appl. Phys. Lett*., 2009, vol. 94, p. 021903.
47. S.G.J. Mochrie, A.M. Mayes, A.R. Sandy, M. Sutton, S. Brauer, G.B. Stephenson, D.L. Abernathy, and G. Grübel: *Phys. Rev. Lett*., 1997, vol. 78, pp. 1275–78.
48. G. Lacroix, T. Pardoen, and P.J. Jacques: *Acta Mater*., 2008, vol. 56, pp. 3900–13.
49. M. Palacios and F. Puertas: *J. Am. Ceram. Soc*., 2006, vol. 89, pp. 3211–21.